Journal of Applied Polymer Science

# Electrochemical Sensing of Glucose Using Polyaniline Nanofiber Dendrites-Amperometric and Impedimetric Analysis

**R. Ramya, M.V. Sangaranarayanan**
Department of Chemistry, Indian Institute of Technology—Madras, Chennai 600036, India
Correspondence to: M.V. Sangaranarayanan (E-mail: sangara@iitm.ac.in)

**ABSTRACT:** A novel electrochemical synthesis of polyaniline (PANI) nanofiber dendrites on platinum electrodes using *p*-toluenesulfonic acid for sensing of glucose is reported. The characterization of PANI is carried out using scanning electron microscopy, transmission electron microscopy, Fourier transform infrared spectroscopy, and ultraviolet (UV)–visible spectral studies. The electrochemical behavior of the PANI-coated electrode is investigated with the help of cyclic voltammetry, chronoamperometry, and impedance spectroscopy, regarding its efficacy as a glucose sensor. The amperometric analysis shows a very low detection limit of ~100 n*M* with the linear regime spanning 50 μ*M*–12 m*M*, while the response time is <5 s. The Michaelis–Menten constant is estimated as 1.24 × $10^{-2}$ M indicating the high activity of the glucose oxidase enzyme. The equivalent circuit fitting of the Nyquist and Bode' plots is carried out to estimate the system parameters. The reliability of the PANI coated electrodes is demonstrated by procuring the authentic samples from the hospitals. The stability and reproducibility of the sensor is also analyzed. © 2012 Wiley Periodicals, Inc. J. Appl. Polym. Sci. 129: 735–747, 2013

**KEYWORDS:** conducting polymers; nanostructured polymers; sensors and actuators

Received 26 July 2012; accepted 25 October 2012; published online 26 November 2012
**DOI: 10.1002/app.38770**

## INTRODUCTION

The development of glucose biosensors constitutes a frontier area of research in the field of sensors and its accurate detection in presence of interfering agents is being extensively analyzed.[1–3] In this context, the efficacy of glucose oxidase has been demonstrated and among several studies pertaining to glucose sensors, mention may be made of the following: (i) use of oxygen as a cosubstrate with generation and detection of hydrogen peroxide[4]; (ii) incorporation of electron-mediators such as ferrocene, quinones, viologens, and so forth[5–7]; and (iii) direct electron transfer between the electrode and the enzyme.[8] The glucose sensors have in general been fabricated by immobilizing the enzyme onto the electrode surface in view of the satisfactory features such as noncontamination and minimal pretreatment. The immobilization of the enzyme can be accomplished using adsorption,[9] attachment through covalent bonding,[10] microencapsulation and entrapment,[11] and so forth.

Although amperometric and potentiometric techniques can be used in general,[12] amperometric sensors seem more promising on account of satisfactory detection limits and enhanced sensitivity. However, at larger potentials, interfering substances such as ascorbic acid (AA) and uric acid (UA), commonly present in biological fluids also get oxidized[13] thus indicating the need for masking the interferences.[14]

Glucose is the main source of energy for the human cells and blood lipids. Hence, it is necessary to quantitatively detect the amount of glucose present in blood, urine, and so forth. The desirable range of glucose is 4.4–6.6 m*M* in blood samples of humans.[1] Further, the continuous noninvasive monitoring of glucose using *in-vivo* and *in-vitro* methods is essential. Also, the fabrication of such sensing devices using nanomaterials is an emerging field due to their unique physical and chemical properties.[15] The use of conducting polymers for sensing of glucose has been investigated during the past few decades, using polypyrrole[16] or polyindole.[17] The advantage of using conducting polymers lies in the fact that the electrochemical synthesis allows direct deposition of the polymer film on the electrode substrate followed by immobilization of biological molecules. The functionality of the conducting polymer enables the covalent linkage of biomolecules. Among a variety of conducting polymers, polyaniline (PANI) is more suitable owing to its good environmental stability, tunable conductivity, and facile synthetic strategies.[18] PANI exhibits four different redox states viz. the leucoemeraldine base (fully reduced form), emeraldine salt

Additional Supporting Information may be found in the online version of this article.

(conducting form, protonated) emeraldine base (de-protonated form), and pernigraniline base (fully oxidized form and non-conducting). The transitions between these forms are due to the redox reactions taking place in the polymer moiety. Furthermore, PANI is stable in diverse solvent media; exhibit desirable electronic properties and strong biomolecular interactions.[19] The sulphonated PANI exhibits satisfactory redox activity even in neutral pH.[20] The different properties of PANI such as pH sensitivity, electrochromism, and conductivity are exploited while fabricating sensors.

Although the earlier reports for synthesis of polyaniline (PANI) dendrites have essentially focused on chemical synthesis, we demonstrate here the electrochemical synthesis of branched PANI nanofiber dendrites. It is of interest to mention that nanostructured PANI offers the possibility of enhanced performance in diverse contexts.[21] The interfacially synthesized PANI nanofibers have been used for sensing gases such as HCl and $NH_3$[22] while those prepared using the metal-organic templates with $FeCl_3$ as the oxidant have been used as a supercapacitor material with a capacitance of 428 $Fg^{-1}$.[23] On the other hand, electrochemically synthesized PANI nanofibers using D and L-camphorsulfonic acid exhibit optical properties.[24] The biofunctionalized PANI nanofiber dendrites have been used for electrochemical immunoassay of biomarkers,[25] while in conjunction with Au nanoparticles, PANI nanofibers can also be used for sensing of sulfur compounds in human breath.[26] In addition, sensing of urea using PANI nanofibers and Pt nanoflowers has also been studied.[27] Hence, it follows that PANI nanofibers possess a wide range of potential applications.

The objectives of this communication are (i) to synthesize PANI nanofiber dendrites on platinum electrodes in presence of *p*-toluene sulphonic acid using potentiodynamic polymerization; (ii) to use the PANI-coated electrode for the sensing of glucose using amperometry and impedance spectroscopy with the help of glucose oxidase enzyme; and (iii) to estimate the Michaelis–Menten constant for ascertaining the catalytic activity of the enzyme.

## EXPERIMENTAL

### Reagents

Glucose oxidase (GOx, EC 1.1.3.4, Type, X-S) from *Aspergillus niger* with an activity of 147,000 $Ug^{-1}$, glucose, UA, AA, and dopamine (DA) were procured from Sigma–Aldrich and used as received. *p*-Toluenesulphonic acid (PTSA) gluteraldehyde, and aniline were obtained from SRL chemicals (India). The solvent *N*-methyl pyrrolidone (NMP) was vacuum distilled and used for the ultraviolet (UV)–visible spectral studies. The Nafion-perfluorinated ionomer was obtained from Sigma-Aldrich as 5 wt % solution and used after dilution to 0.5%. The monomer was distilled twice before each experiment and triple-distilled water was used in all experiments. The buffer solution was prepared from phosphate-buffered saline (PBS, Sigma). Glucose stock solutions were stored overnight before use. All the experiments were carried out at 25°C, unless otherwise specified.

### Electrochemical Studies

The cyclic voltammetric, amperometric, and impedance measurements were performed using the electrochemical workstation CH 660 A (CH Instruments, USA). The working electrode was Pt with a diameter of 2 mm (CH Instruments) while the reference electrode was a saturated calomel electrode (SCE), Pt wire being the counter electrode (CH Instruments) in a three-electrode arrangement. In the case of impedance and amperometric experiments, the working electrode is designated as Pt/PANI-nfbD/GOx/Nf indicating the coating of PANI nanofibres on Pt in presence of Nafion.

### Fourier Transform Infrared, UV–Visible Spectra, XRD, SEM, and TEM Studies

The Fourier transform infrared (FT-IR) spectra (in NMP solvent) were obtained from the Perkin-Elmer spectrophotometer (Spectrum one).The SEM and TEM measurements were made using Philips FEI Quanta 200 and JEOL JEM 2100, mounting the samples on a carbon tape and carbon coated copper grid, respectively. The UV–vis spectra were obtained using the Perkin-Elmer Cary 5E UV–VIS-NIR spectrophotometer. The X-ray diffraction (XRD) patterns were obtained using BrukerD8 Advance equipped with Cu $K_\alpha$ instrument ($\lambda = 1.54$ Å).

### Preparation of Pt/PANI-nfbD/GOx/Nf Electrode

The platinum electrode is polished to a smooth finish using various grades of alumina powders from 0.05–0.30 μm followed by ultrasonication of the electrode for 15 min. The PANI-coated Pt electrode is prepared by polymerizing 0.03*M* aniline in 0.5*M* PTSA using cyclic voltammetry at a scan rate of 100 mV $s^{-1}$ for 20 cycles. This electrode is then repeatedly washed with methanol and distilled water. A solution containing 0.5 mg $mL^{-1}$ GOx was prepared with 5% gluteraldehyde in a PBS 7 solution and 5 μL of this mixture was drop-casted onto the Pt/PANI electrode and allowed to cross link for 4 h. Subsequently, the electrode is washed with distilled water and PBS 7 to eliminate any loosely bound enzyme and finally 0.5 wt % of Nafion was doubly-coated and allowed to dry at 25°C for about an hour. This electrode (Pt/PANI-nfbD/GOx/Nf) is used for sensing of glucose.

### Amperometric Studies

The amperometric measurements are carried out using phosphate buffer (pH 7) supporting electrolyte in an electrochemical cell provided with the magnetic stirrer. After several repeated trials, the optimal potential was chosen as 0.5 V and the steady state current is recorded each time.

### Electrochemical Impedance Spectroscopy Measurements

The estimation of glucose is also carried out with the help of electrochemical impedance spectroscopy (EIS) measurements of the coated electrode in an unstirred e solution containing PBS (pH 7) solution. The operating DC potential is chosen as 0.4 V with the frequency range of 1–$10^5$ Hz and amplitude of 5 mV.

## RESULTS AND DISCUSSION

### Cyclic Voltammetric Studies

Figure 1 depicts the multicycle voltammogram for the electropolymerization of aniline on Pt electrode using 0.03*M* aniline and 0.5*M* PTSA at a scan rate of 100 mV $s^{-1}$. The first oxidation peak in PANI which appears at 0.2 V is due to the oxidation of leucoemeraldine state to the more conducting emeraldine structure. The variation of $i_p$ with $v^{1/2}$ is carried out

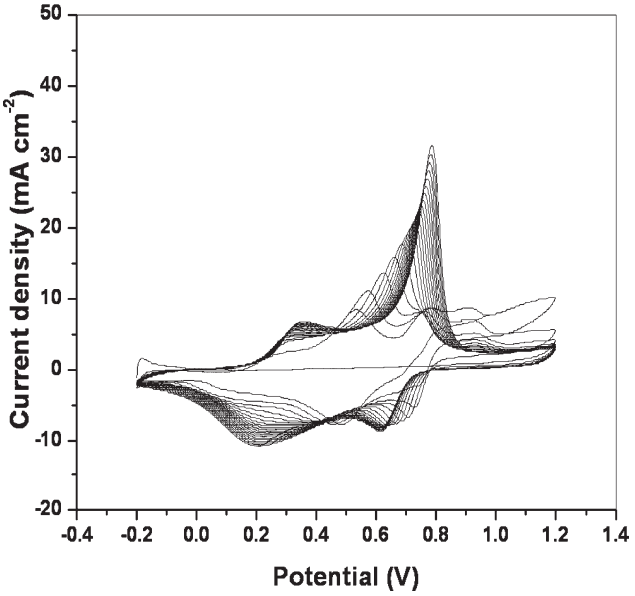


**Figure 1.** Multicycle voltammogram depicting the electropolymerization of aniline on Pt from 0.03 *M* aniline+0.5 *M* *p*-PTSA at a scan rate of 100 mV $s^{-1}$. The potential is scanned from −0.2 V to 1.2 V while the number of cycles is 20.

for the first oxidation peak to ensure the reversibility of the polymer. The emeraldine peak shifts to more positive potentials, subsequently yielding a single peak. The current density increases with the number of cycles which indicates the transition of emeraldine to pernigraniline form as well as the uniform growth of the PANI layer. The peak current ($i_p$) depends linearly on the square root of scan rate ($v^{1/2}$) as shown in Figure 2, indicating the diffusion-controlled process. PTSA is capable of directing the oriented growth of PANI[28]; further on account of its functioning as a dopant as well as a soft template, PTSA is especially suited for diverse applications.[29]

### Microscopic Studies and Thickness Measurements

The scanning electrochemical microscopy (SEM) and transmission electron microscopy (TEM) images depicted in Figures 3 and 4 reveal the presence of the PANI nanofiber dendrites. Further, a relatively uniform distribution of PANI nanofiber dendrites with diameters ranging from ~50–300 nm and lengths of 2–5 μm is noticed. At higher magnifications, the clarity got reduced in the SEM image of Figure 3(C) on account of low resolution; nevertheless, the SEM images indicate the occurrence of nanofibers dendrites without using any surfactants or sophisticated experimental protocols. The TEM images indicate the evolution of PANI nanoparticles in a three-dimensional manner while forming the PANI nanofiber dendrites as shown in Figure 4. Because the electron beam was of high energy, the polymer film starts to disintegrate after prolonged exposure. PANI prepared by chemical polymerization of aniline using hexadecyl trimethylammonium chloride in acetic acid solution has also yielded dendritic nanofiber morphology.[30] Such a fibrous structure is suitable for the immobilization of enzymes through intercalation and consequently for the detection of glucose via the GOx enzyme. This nanofiber morphology of PANI enables excellent crosslinking between the enzyme and polymer, thus enhancing the sensitivity of the electrode for analytical purposes.

The thickness of the PANI coating is measured using SEM measurements (Figure 5). The film thickness could not be measured using the optical profilometer because the thickness of PANI layer is large, the film being opaque. Hence, the roughness of the electrode is estimated using the perthometer as ~0.04 μm. The thickness values deduced from SEM images

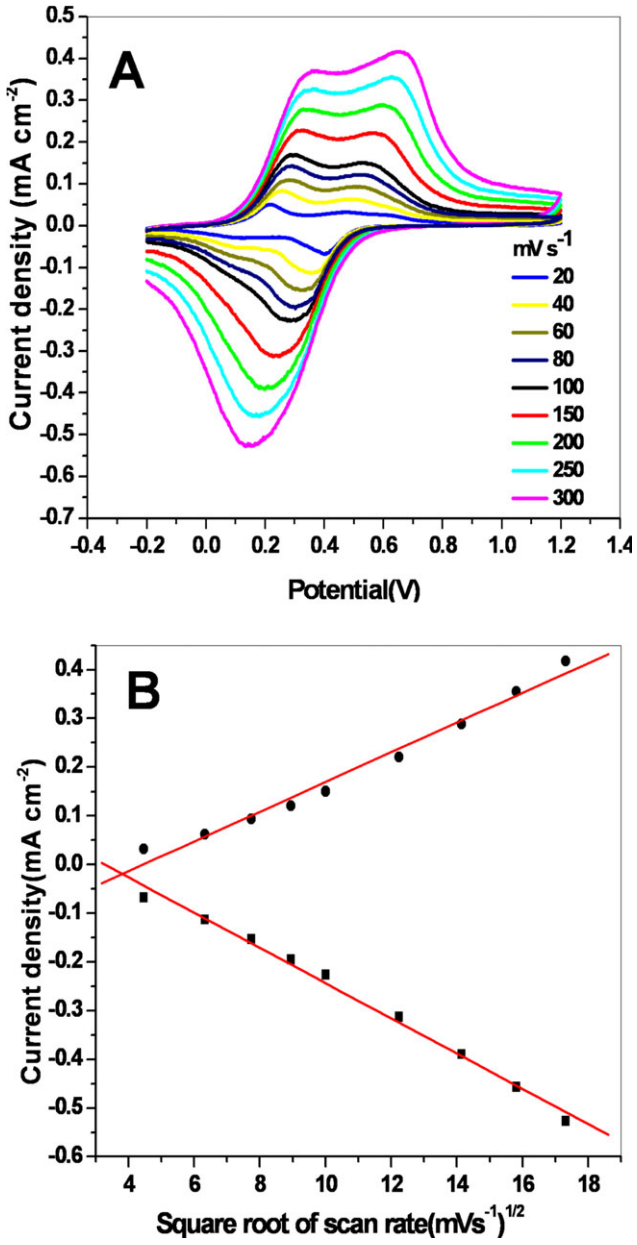


**Figure 2.** (A) Cyclic voltammograms of the PANI-deposited Pt electrode in 0.5 *M* PTSA electrolyte at various scan rates (20, 40, 60, 80, 100, 150, 200, 250, and 300 mV $s^{-1}$). (B) The variation of the anodic (●) and cathodic (■) peak currents with the square root of scan rates. [Color figure can be viewed in the online issue, which is available at wileyonlinelibrary.com.]

Applied Polymer SCIENCE

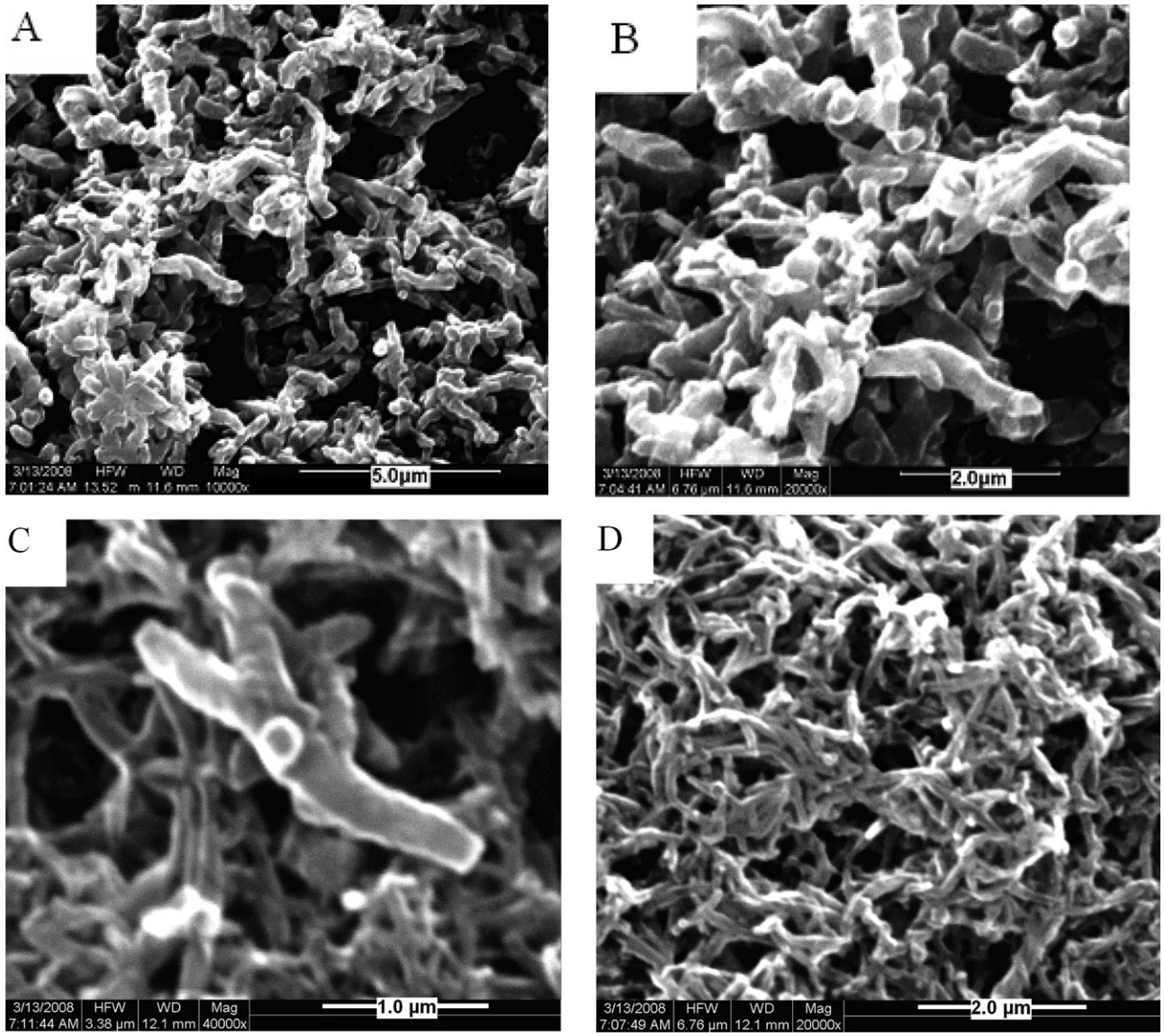


**Figure 3.** The SEM images of PANI at different magnifications (A) 10,000; (B) 20,000; (C) 40,000, and (D) 20,000 depicting the dendritic, fibrous structures.

pertaining to the polymerization for 10 and 50 cycles are, respectively, ~96.8 and ~376.3 nm. Because the roughness factor is larger than the film thickness, no fringes are seen in optical profilometer and hence a perthometer is more suitable for estimating the roughness.

### FTIR, UV, and XRD Analysis

The FT-IR spectrum in Figure 6(A) depicts the typical absorption bands at 1505 $cm^{-1}$ and a shoulder at 1471 $cm^{-1}$ which are due to the backbone ring vibrations of PANI. The band at 1679 $cm^{-1}$ arises due to the carbonyl stretching vibration of the NMP solvent. The absorption bands at 1173 $cm^{-1}$ [$\nu$(C—N) in B—$NH^{+}$–Q], 1300 $cm^{-1}$ [$\nu$ (C—N)], 1427 $cm^{-1}$ [$\nu$ (C—N) in N—B—N] and 1505 $cm^{-1}$ [$\nu$ (C—N) in N=Q=N] appear as very strong bands (where B and Q represent benzenoid and quinoid moieties). The ratio N=Q=N absorption: N—B—N absorption is a measure of the extent of oxidation in the emeraldine form of the polymer while the ratio B—$NH^{+}$—Q absorption: N=Q=N absorption provides the extent of protonation of imine nitrogen atoms in the polymer,[31,32] The shift in the benzenoid as well as quinoid absorption vibrations is toward lower frequencies and is characteristic of protonated PANI.[33]

### UV–Visible Spectra

The typical peaks appearing at 342, 424, and 865 nm in the UV–visible spectrum correspond to the emeraldine salt form of PANI. The absorption bands at 342 nm arise due to the $\pi$-$\pi^{*}$ electron transition within the benzenoid segment and the absorption bands having a local maximum at 424 and 865 nm are related to the protonation of the polymer backbone and formation of polarons, respectively. The peaks pertaining to the emeraldine base form occur at 335 and 642 nm and are attributed, respectively, to the $\pi$-$\pi^{*}$ transitions of the phenyl ring and the exciton transition (n- $\pi^{*}$ transition).[34] In the present study,

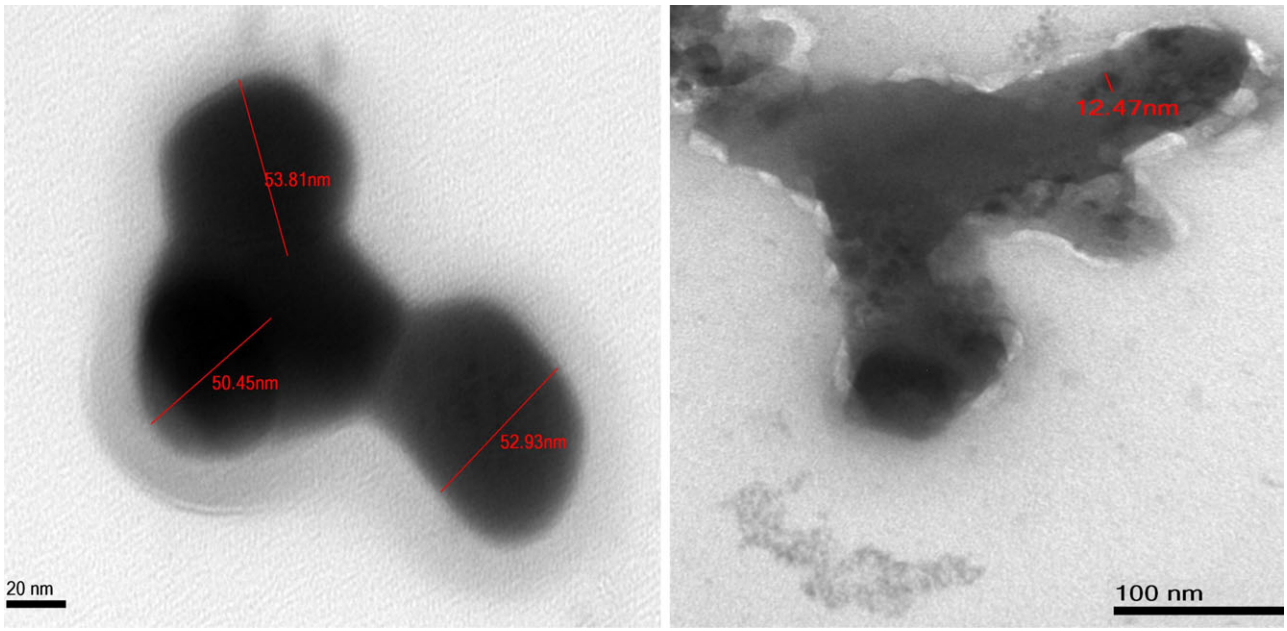


**Figure 4.** The TEM images of PANI depicting the three-dimensional growth of nanofiber dendrites. [Color figure can be viewed in the online issue, which is available at wileyonlinelibrary.com.]

the emeraldine base peaks for PANI at 335 and 638 nm are noticed [Figure 6(B)].

XRD studies

The appearance of a broad peak in the XRD pattern of Figure 7 reveals the amorphous nature of the PANI nanofiber dendrites. The peak for PANI obtained here with PTSA dopant arises at higher $2\theta$ values in comparison with PANI synthesized using other dopants.[35] Hence, a stronger interaction between the PANI and PTSA is inferred here. Furthermore, electrochemical techniques for the synthesis of PANI in general yield amorphous structure.[36]

### Mechanism of Glucose Sensing

The sensing of glucose involves the mechanism wherein the GOx enzyme leads to the oxidation of glucose while itself getting reduced. This reduced form gets regenerated via reoxidation by $O_2$ in the solution, subsequently forming $H_2O_2$, the amount of which is a direct measure of the concentration of glucose.[37] Hence, the current increases with the concentration of glucose but reaches a plateau. PANI acts as a matrix for the effective immobilization of glucose oxidase enzyme in the nanofiber dendrite structure. A simplistic representation of the role of GOx is as follows:

$$\beta - \text{glucose} + O_2 \xrightarrow{GO_X} \beta - \text{gluconicacid} + H_2O_2 \quad (1)$$

$$H_2O_2 \rightarrow O_2 + 2H^+ + 2e^- \quad (2)$$

### Amperometric Measurements

To analyse the effect of the polymerization cycles, the deposition of PANI was also carried out with various cycles ranging from 5 to 30. The corresponding amperometric data acquired with PBS 7 at 0.5 V indicated no appreciable change in current density with addition of glucose, when the cycle number was 5 and 10. When the number of polymerization cycles is 20, the magnitude of the current density obtained is higher and the linear regime gets extended to larger concentrations. However, when the number of cycles increases beyond 30, despite a larger magnitude of current, the linear regime becomes lower; this may be due to the dense PANI dendritic layer crowding the electrode surface. Consequently, the number of polymerization cycles is fixed at 20 which yields the linear relation till 12 m*M*. The

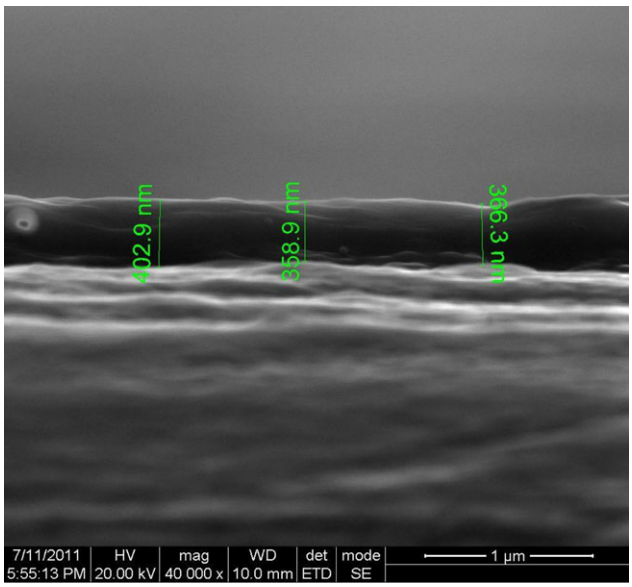


**Figure 5.** Typical SEM image of PANI-coated Pt electrode indicating the thickness of the film with the number of polymerization cycles being 50. [Color figure can be viewed in the online issue, which is available at wileyonlinelibrary.com.]

Applied Polymer SCIENCE

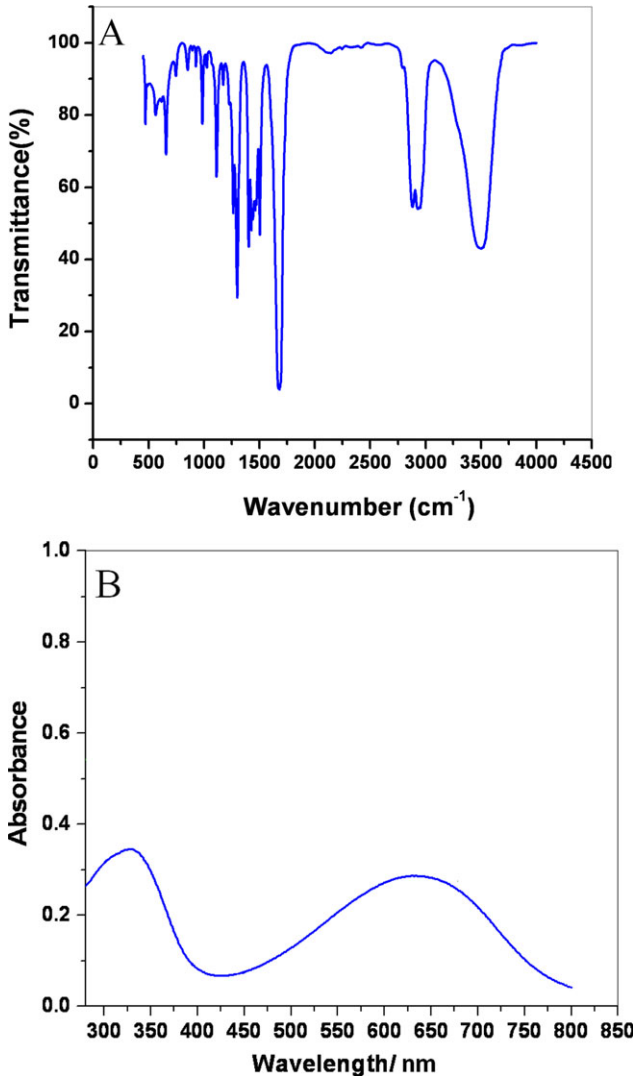


**Figure 6.** (A) FT-IR spectrum of PANI-nanofiber dendrites in the presence of NMP as solvent and (B) UV–visible spectrum of PANI-nanofiber dendrites indicating the n-$\pi^*$ and $\pi$-$\pi$ * transitions. [Color figure can be viewed in the online issue, which is available at wileyonlinelibrary.com.]

sensor is able to sense very low levels of glucose (100 n*M*), and the linearity was observed from 50 μ*M* till 12 m*M*. The factors to be considered in quantifying the limits of detection include instrumental noise, matrix effects, and interferences. Figure 8 depicts the performance of the electrode with and without Nafion coating. Although the electrode without Nafion coating exhibits higher current density, it is also prone to interferences from AA and UA.

The unique feature of PANI is that it is stable in air and has a large shelf life. The amperometric response of Pt/PANI-nfbD/GOx/Nf is measured at various potentials and the optimum potential yielding a high current density is found to be 0.5 V vs. SCE. Figure 9 depicts the variation of the current density with the concentration of glucose and the linear relation is noticed till 12 m*M* and is higher than the range obtained using $SiO_2$ nanoparticles[38] and Pt microparticles.[39] The sensitivity of

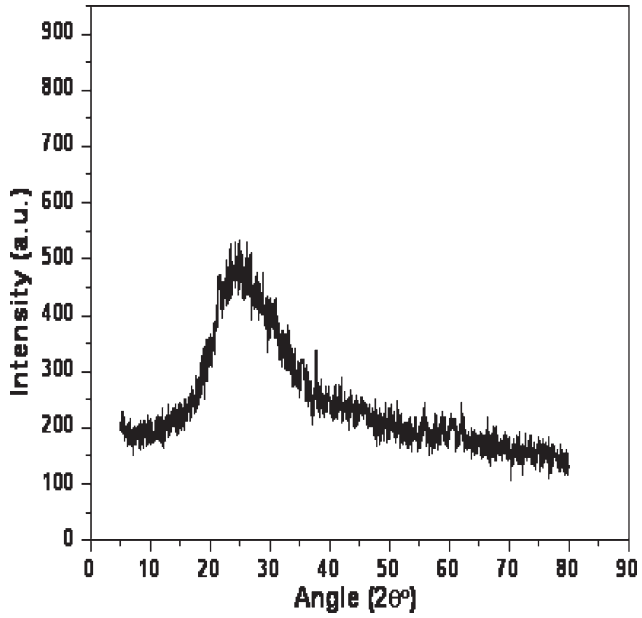


**Figure 7.** The XRD spectrum of PANI nanofiber dendrites indicating the amorphous nature of the nanofibers.

Pt/PANI-nfbD/GOx/Nf electrode as estimated from Figure 9(B) is 166 μAcm$^{-2}$ m$M^{-1}$. The efficiency of the PANI nanofiber dendrites in sensing glucose is attributed to the activity of enzyme confined within the nanofiber structure, which has a high surface area in contrast to the normal globular structure of PANI.

This higher sensitivity in comparison with other PANI involving PANI/Polyisoprene[40] and PANI/poly(vinyl sulphonate)/GOD[41] and Pd-$TiO_2$[42] may arise from (i) the facilitated electron

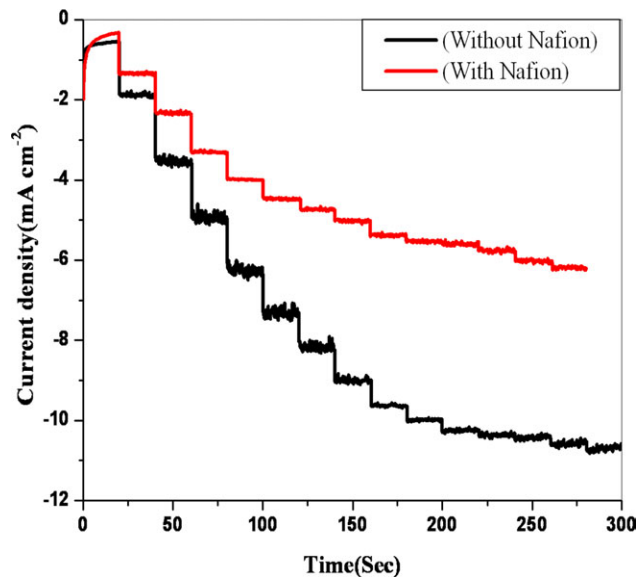


**Figure 8.** Chronoamperometric response of the Pt/PANI-nfbD/GOx electrode in 100 m*M* of pH 7.0 PBS in the presence and absence of Nafion coating, with successive additions of 1 m*M* glucose at a constant potential of 0.5 V. The stirring rate is 300 rpm. [Color figure can be viewed in the online issue, which is available at wileyonlinelibrary.com.]

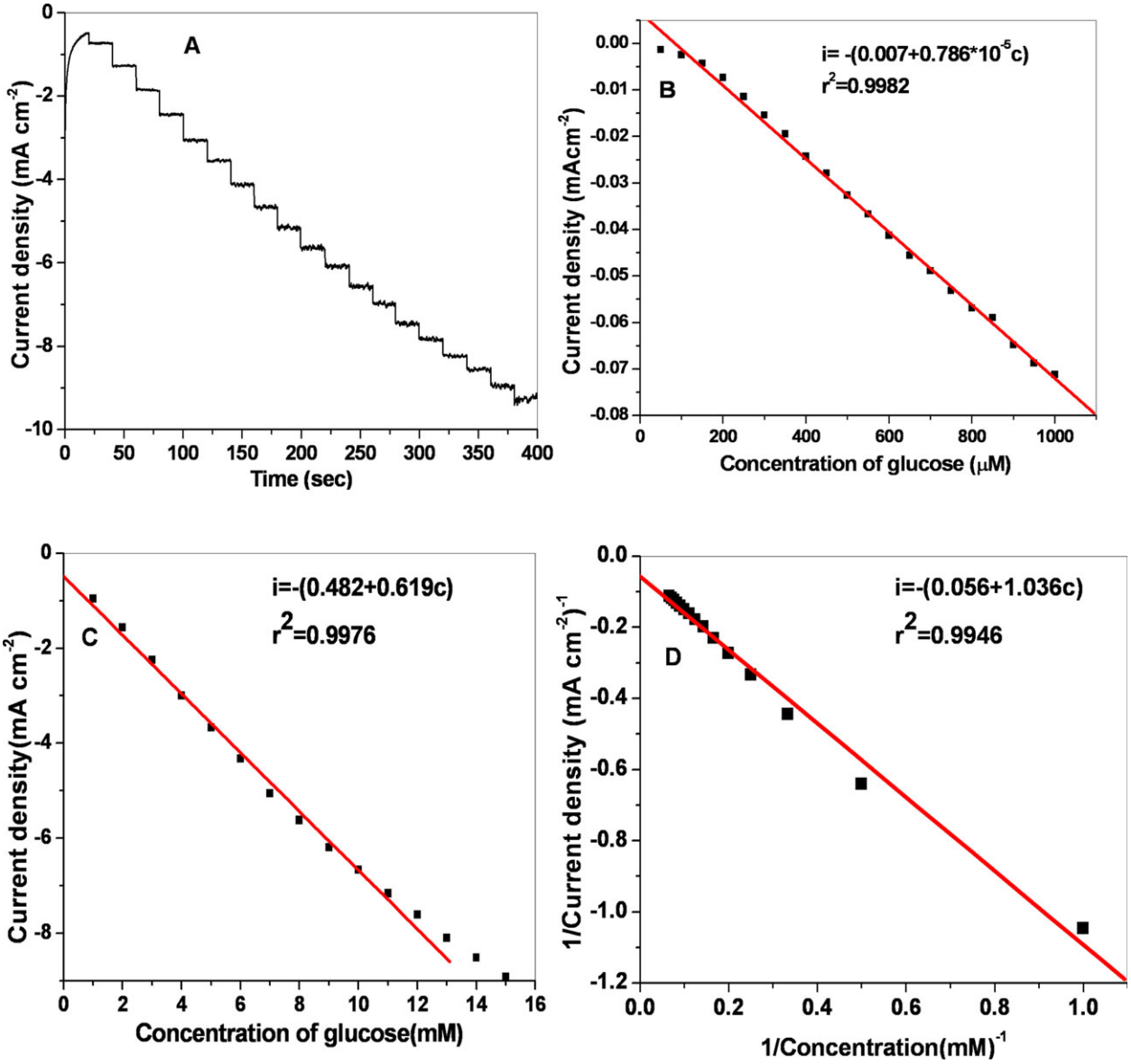


**Figure 9.** (A) Amperometric response of the Pt/PANI-nfbD/GOx/Nf electrode in 100 m*M* of pH 7.0 PBS, with successive additions of 1 m*M* glucose. (B) Calibration graph for 100–1 m*M* concentration; (C) calibration graph for 1–16 m*M* concentration range, and (D) Typical Lineweaver-Burk plot (In the regression equation, i and c are given for brevity instead of 1/i and 1/c). [Color figure can be viewed in the online issue, which is available at wileyonlinelibrary.com.]

transfer involving only PANI and GOx and (ii) the nanofiber morphology of PANI resulting in satisfactory enzyme loading. The detection limit of glucose is estimated as 100 n*M* based on the signal to noise ratio of 3.

To evaluate the biological activity of the immobilized enzyme, it is customary to use the apparent Michaelis–Menten constant $K_M$ using the equation

$$\frac{I_{max}}{I_s} = \frac{K_M}{C} + 1 \quad (3)$$

where $I_s$ denotes the steady state current and $I_{max}$ is the maximum current, C being the concentration of the glucose. With the help of the Lineweaver–Burk plot shown in Figure 9(C), the values of $K_M$ and $I_{max}$ are deduced, respectively, as 12.4 m*M* and 2.88 mA $cm^{-2}$. $K_M$ value indicates that the immobilized GOx possesses a good enzymatic activity *vis a vis* a high affinity for glucose. The value of $K_M$ is lower than that reported for GOx in the case of PANI/Graphite (16.6 m*M*) and PANI/Prussian Blue (28.8 m*M*).[43,44] The lower value of $K_M$ indicating a satisfactory sensitivity arises from fast electron transfer activity, and good synergy between PANI and GOx. Table I provides typical $K_M$ values pertaining to glucose biosensors using PANI and polypyrrole as conductive matrices.

The comparison of other sensing systems for glucose with the present Pt/PANI-nfbD/GOx/Nf electrode is shown in Table II.

Applied Polymer SCIENCE

**Table I.** The Michaelis–Menten Constants $K_M$ for Glucose Biosensors Pertaining to a Few Conducting Polymers

| System | $K_M$ (m*M*) | References |
|---|---|---|
| PANI/graphite composite | 16.57 | 43 |
| Pt/GOD-PANI/PB | 22.70 | 44 |
| PPy/PA/GOx | 5.50–11.00 | 45 |
| PTED/GOx/Pt | 15.70 | 46 |
| PANI/Ionic liquid | 31.59 | 47 |
| Pt/PANI nanocomposite/BDD | 4.10 | 48 |
| PANI(NT)/PGLD;CHD-GOx | 7.50; 6.30 | 49 |
| NS-PANI/GOx/ITO | 2.10 | 10 |
| N-subsPpy/GOx | 25.95; 28–33 | 50 |
| Pt/Ppy/GOx | 28–33 | 51 |
| Pt/PANI-nfbD/GOx/Nf | 12.4 | Present work |

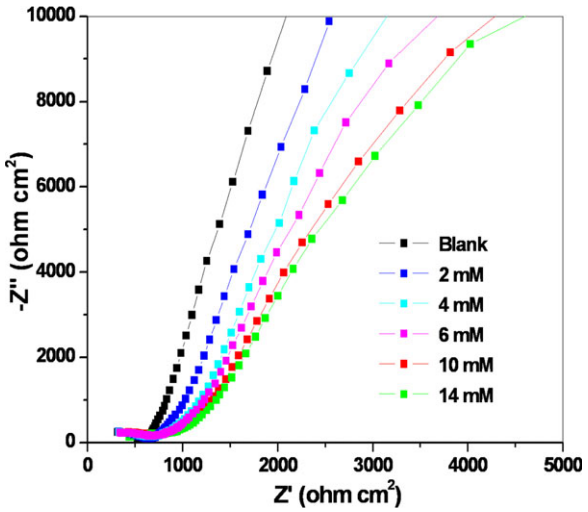


**Figure 10.** Nyquist plots of Pt/PANI-nfbD/GOx/Nf electrode in 100 m*M* of PBS pH 7.0 with successive additions of glucose at concentrations ranging from 2–14 m*M*. The electrode was biased at a potential of 0.4 V with an amplitude of 5 mV. [Color figure can be viewed in the online issue, which is available at wileyonlinelibrary.com.]

### EIS Analysis

To obtain a comprehensive analysis of the impedance data, it is preferable to construct Nyquist and Bode' plots. Figure 10 depicts the Nyquist plots for the Pt/PANI-nfbD/GOx/Nf electrode for various concentrations of glucose. The customary semicircles at high frequencies, followed by a slanting line in the low frequency regions due to the diffusion-limited electron transfer are noticed. The diameter of the semicircle denotes the charge transfer resistance ($R_{ct}$).[59] To correlate the EIS data with the physiochemical properties of the system, it is imperative to construct the equivalent circuit of the system and interpret the derived parameters. The charge profile close to the interface constitutes the electrical double layer whose capacitance is denoted as $C_{dl}$. Furthermore, the diffusion layer constituting the reaction zone is described in terms of a corresponding impedance—a combination of the charge transfer resistance ($R_{ct}$) and capacitance constant-phase element (CPE) in series. The latter incorporates the inhomogeneity of the electrode while $R_s$ denotes the resistance arising from the electrolyte solution. The solution resistance ($R_s$) is dictated by the ions in the solution. As the oxidation of glucose occurs, the overall charge distribution and the mobility of ions at the diffusion layer get altered, thereby influencing the $R_{ct}$ and CPE parameters.

The real and imaginary parts of the impedance increase with concentration of glucose and the increase is more pronounced from frequencies above $R_{ct}$ to frequencies <10 Hz. The GOx acts as a catalyst for the oxidation of glucose, the product of which creates an insulating film on the electrode. This increases the charge transfer resistance $R_{ct}$ significantly. The variation of the charge transfer resistance is associated with the blocking behavior of the electrode. Although the charge transfer resistances can be correlated[60] with the concentration of the analyte (glucose), the calibration curve is constructed here using (i) the real part of impedance(Z') in the Nyquist plot[61,62] and (ii) the |Z| values from the Bode' magnitude plot.[63]

In the present case, this variation at a frequency of 9.766 Hz is analyzed, although any other frequency above the charge transfer resistance ($R_{ct}$) can also be chosen. For quantitative estimations using impedance data, the charge transfer resistance is found to be less sensitive than the nonfaradaic region

**Table II.** Comparison of the Performance of Various Glucose Sensing Materials with Pt/PANI-nfbD/GOx/Nf Electrode

| System | Linear range (m*M*) | LOD (μM) | Sensitivity ($\mu AmM^{-1}\ cm^{-2}$) | $K_M$ (mM) | Response time (s) | Stability | References |
|---|---|---|---|---|---|---|---|
| GOx/Pt/MWCNT/PANI | 0.003–8.2 | 1.0 | 16.10 | 0.64 | <5 | 90% (2 days) | 52 |
| Cu nanocluster/MWCNT/GCE | 0.0007–3.5 | 0.21 | 17.76 | - | 5 | - | 53 |
| Pt/PANI/BDD | 0.0059–0.514 | 0.102 | 5.54 | 4.076 | - | 80% (40 days) | 48 |
| Gox/nano-PANI/GC | 0.01–1 | 0.5 | - | 1.05 | 5–10 | 93% (2 weeks) | 54 |
| Pt/GOD-PANI/PB | ~8 | - | 1.90 | 22.7 | - | 85% (24 h) | 44 |
| Au-nano/PANI/GOx | 0.001–0.8 | 0.5 | 2300 | - | <5 | 95% (2 weeks) | 55 |
| Nf-silica/MWCNT-g-PANI/GOx | 1–10 | 0.1 | 5.01 | - | ~6 | 93% (20 days) | 56 |
| Au-g-PANI-c-(CS-CNTs)-GOD | 1–20 | 0.1 | 16.50 | 5.35 | 5–10 | 97% (20 days) | 57 |
| PANI-NW/GOx/CC | 0–8 | 0.05 | ~2500 | - | - | 82% (1 week) | 58 |
| Pt/PANI-nfbD/GOx/Nf | 0.05–12 | 0.1 | 166 | 12.4 | <5 | 89% (30 days) | Present work |

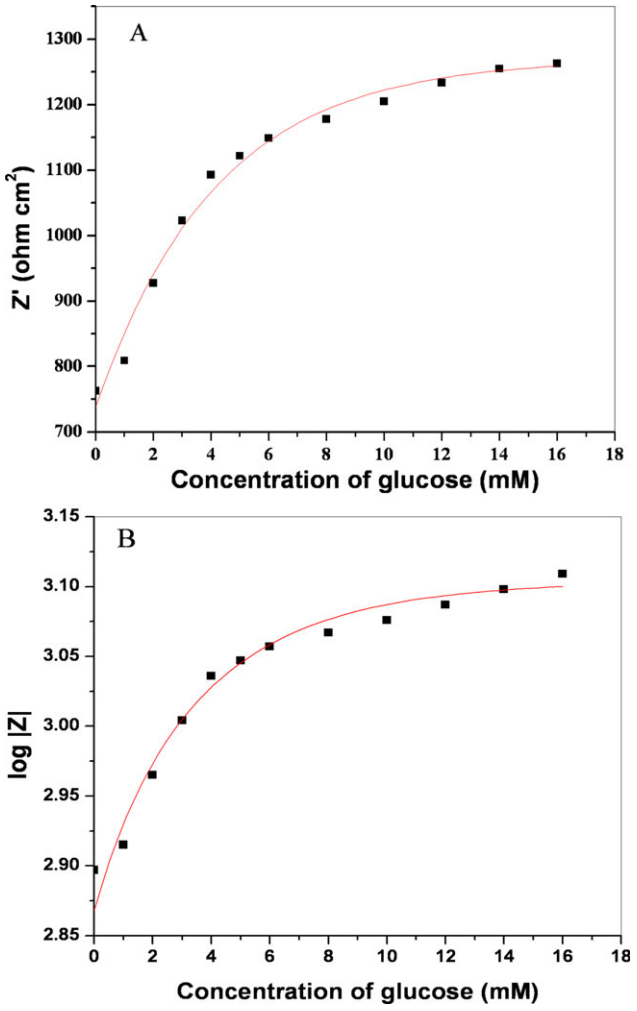


**Figure 11.** Calibration curve for Pt/PANI-nfbD/GOx/Nf electrode obtained from (A) Nyquist and (B) Bode' magnitude plots for various concentrations of glucose at 9.766 Hz. The points denote the experimental data and the lines are drawn as a guide to the eye. [Color figure can be viewed in the online issue, which is available at wileyonlinelibrary.com.]

as was found in an earlier study using Au nanoparticle-peptide films.[64]

As can be seen from the calibration curve depicted in Figure 11, the real part of the impedance increases with the addition of the glucose and is attributed to the enhanced double layer resistance. The linear regime is noticed till about 6 m*M*. The quantitative analysis of the EIS data requires formulating an equivalent circuit and the circuit depicted in Figure 12 reproduces the Nyquist and Bode' plots satisfactorily in the linear regime. This circuit consists of the solution resistance ($R_s$), charge-transfer resistance ($R_{ct}$), and two CPE's denoted as

$$Z_{CPE1} = (j\omega)^{-n}1 \rightarrow /A_1 \quad (4)$$

$$Z_{CPE2} = (j\omega)^{-n}2 \rightarrow /A_2 \quad (5)$$

wherein the exponents $n_1$ and $n_2$ denote the capacitive or resistive nature of the electrode.[65] The terms $Z_{CPE1}$ and $Z_{CPE1}$ denote the impedance arising from the constant phase elements while $A_1$ and $A_2$ are constants which become equal to $C_{dl}$ when $n_1 = n_2 = 1$ and $\omega$ denotes the angular frequency. The constant phase element has been used here instead of a pure capacitor so as to incorporate the nonideal nature of the capacitance arising from inhomogeneity of the electrodes coated with conducting polymers.[66]

The typical fitting of the impedance data pertaining to 8 m*M* concentration of glucose using MATLAB programming is depicted in Figure 13 for the Nyquist, Bode' magnitude and Bode' phase angle plots. The calibration curves obtained using (i) the Nyquist plot to construct Z' vs. the concentration and (ii) the Bode' magnitude plots to construct |Z| vs. concentration are almost identical and the linear range calculated from the two methods is till ~6 m*M*. The customary fitting of the Nyquist plots alone are not adequate in general to interpret the impedance data. Hence, in the present analysis, the Bode' plots have also been reproduced with the circuit postulated in Figure 12. In fact, the equivalent circuit is more sensitive to the fitting of the Bode' plots.

The fitting of the impedance data to the equivalent circuit represented in Figure 12 yields the system parameters provided in Table III. These values indicate that the Pt/PANI-nfbD/GOx/Nf electrode possesses highly capacitive nature and the electron transfer between the PANI and the enzyme moiety is a favorable one.

The charge transfer resistance ($R_{ct}$) increases with concentration of glucose and is attributed to the formation of an insulating film. The $CPE_1$ is nearly constant indicating that the double layer characteristics remain the same. On the other hand, the systematic increase in $CPE_2$ is interpreted as due to the increase in charge transfer resistance with increase in the concentration of glucose. This variation of $R_{ct}$ and $CPE_2$ is consistent with the variation of the diffusion layer thickness with surface concentrations of glucose and this value is lower in comparison to the $R_{ct}$ values of PANI synthesized using ionic liquid.[47] Although the impedance data provides complete information regarding the behavior of the electrochemical system, its usefulness in analyzing the effect of interfering agents is limited, since in this case, the interpretation of the derived circuit parameters becomes tedious. Hence, at the present stage of analysis, amperometry is more preferable for analyzing the effect of interfering agents. The listing of the MATLAB program is provided in the Supporting Information.

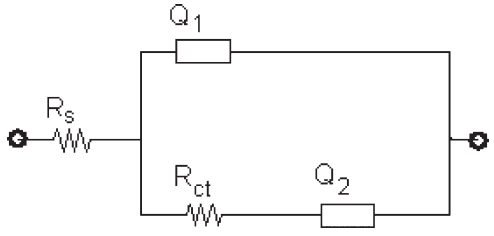


**Figure 12.** The equivalent circuit of the Pt/PANI-nfbD/GOx/Nf electrode in 100 m*M* of PBS pH 7, for fitting of the impedance data.

Applied Polymer SCIENCE

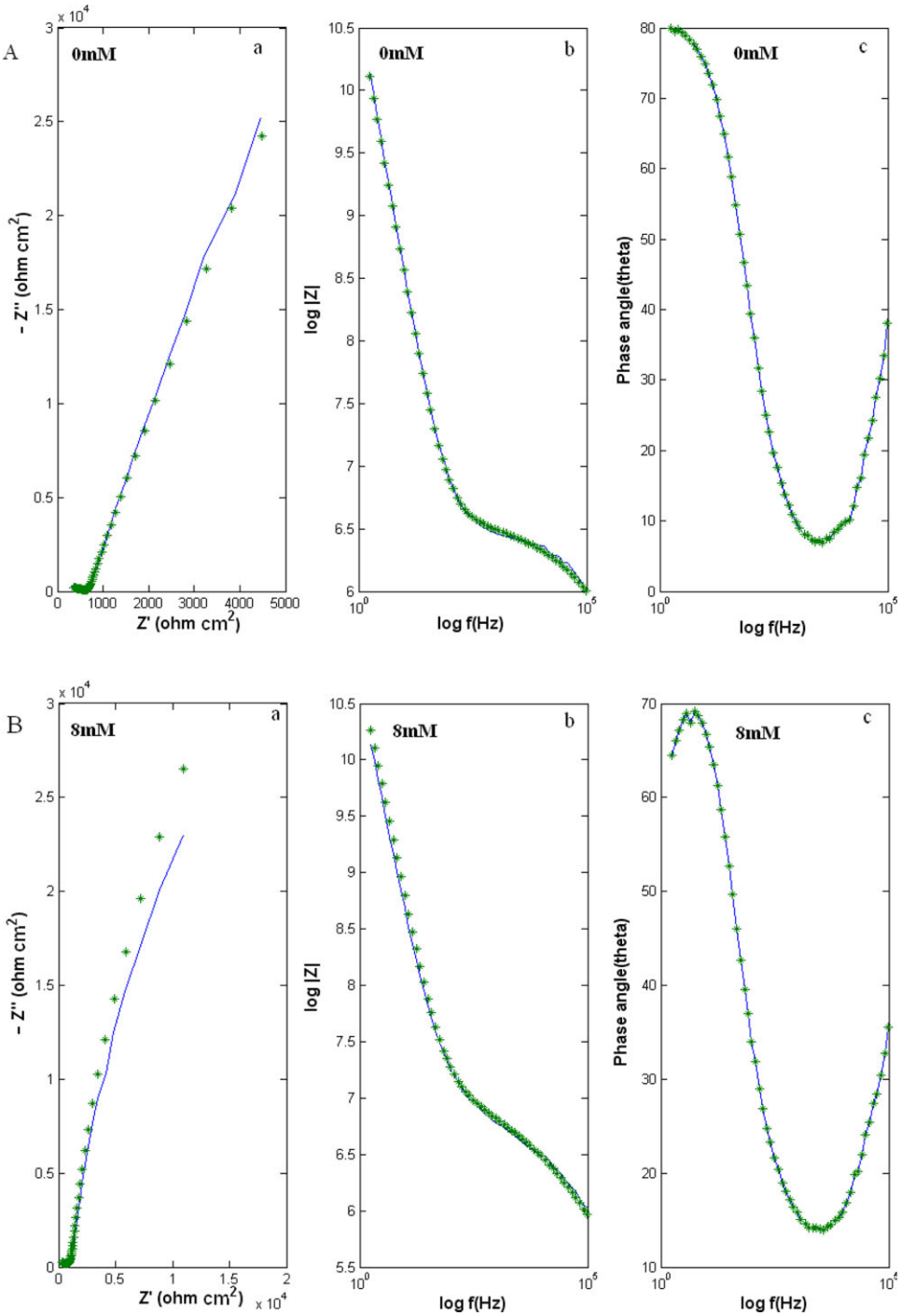


**Figure 13.** Typical impedance spectra of Pt/PANI-nfbD/GOx/Nf electrode in 100 m*M* of PBS pH 7 for 0 and 8 m*M* concentrations of glucose (a) Nyquist;(b) Bode' magnitude; and (c) Bode' phase angle plots in the frequency range $10^5$–1 Hz. The electrode was biased at a potential of 0.4 V vs. SCE with perturbation amplitude of 5 mV. The points denote the experimental data while the lines are obtained by fitting of the data for the equivalent circuit depicted in Figure 12. [Color figure can be viewed in the online issue, which is available at wileyonlinelibrary.com.]

### Effect of Temperature and Potential

To obtain the satisfactory sensitivity and detection limits, the applied potential of Pt/PANI-nfbD/GOx/Nf electrode needs to be optimized. The effect of potential on the current density is depicted in Figure 14. Because the maximum current density is obtained at a potential of 0.5 V vs. SCE, this value is chosen for the sensing of glucose. However, this potential also represents the region wherein the interfering agents such as AA, UA, acetaminophen, and so forth yield the electrochemical response. To overcome this limitation,[67] a double coating of 0.5% Nafion on the electrode surface has been used such that it acts as a barrier for the interfering agents.

**Table III.** The System Parameters for the Nyquist and Bode' Plots of Pt/PANI-nfbD/GOx/Nf Electrode Pertaining to the Equivalent Circuit Depicted in Figure 12 in the Linear Concentration Regime

| Concentration (m*M*) | $R_s$ (ohm cm$^2$) | $R_{ct}$ (ohm cm$^2$) | $CPE_1$ ($10^{-7}$ ohm$^{-1}$ cm$^{-2}$ s) | $n_1$ | $CPE_2$ ($10^{-5}$ ohm$^{-1}$ cm$^{-2}$ s) | $n_2$ |
|---|---|---|---|---|---|---|
| 0 | 105 ± 2 | 581 ± 4 | 0.90 ± 0.02 | 0.74 ± 0.01 | 0.40 ± 0.10 | 0.90 ± 0.01 |
| 1 | 105 ± 3 | 550 ± 2 | 0.90 ± 0.03 | 0.76 ± 0.02 | 0.50 ± 0.10 | 0.86 ± 0.02 |
| 2 | 105 ± 1 | 580 ± 10 | 0.90 ± 0.01 | 0.76 ± 0.02 | 0.55 ± 0.03 | 0.86 ± 0.01 |
| 4 | 106 ± 0.5 | 620 ± 1 | 0.90 ± 0.05 | 0.75 ± 0.03 | 0.60 ± 0.05 | 0.83 ± 0.01 |
| 8 | 107 ± 0.5 | 695 ± 1 | 0.90 ± 0.01 | 0.71 ± 0.01 | 0.90 ± 0.02 | 0.81 ± 0.01 |

Figure 15 depicts the temperature dependence of the Pt/PANI-nfbD/GOx/Nf electrode in PBS 7 buffer. The influence of the temperature on the glucose sensor is more subtle. Although the enzymatic activity decreases with increase in temperature, the rate of the electrochemical reaction increases with increase in temperature. Consequently, an optimum temperature needs to be ascertained. As shown in Figure 15, the current density for oxidation of glucose is maximum at about 25°C.

### Interference Studies

The interference from other electroactive species such as UA, AA, DA, and so forth needs to be analyzed because these compounds may coexist with glucose in the blood serum. Figure 16(A) depicts the effect of interfering agents on the performance of the Pt/PANI-nfbD/GOx/Nf electrode pertaining to the detection of glucose with and without Nafion coating. The Pt/PANI-nfbD/GOx/Nf electrode response for the concentration of 0.5 m*M* each of UA and DA yielded no current while AA produced a slight but negligible current response, but in the absence of Nafion, the coated electrode yields high response for AA as well as glucose and a moderate response for UA and DA. Hence, the Nafion coating plays a crucial role in inhibiting the interferences. Because Nafion prevents the interference from AA, UA, and so forth, a highly selective response to glucose is obtained with the double coating of Nafion (0.5 wt %) without using enzyme preoxidation or restriction to low potentials.

To analyze the influence of interfering agents in sensing of glucose using impedance studies, Nyquist plots are constructed [Figure 16(B)] separately for blank solution (buffer + 0.5 m*M* glucose) and subsequently with 0.5 m*M* UA, 0.5 m*M* DA, and 0.5 m*M* AA. Although there is a shift of the charge transfer resistance ($R_{ct}$) in each case, its quantification will require a different equivalent circuit and further studies are needed to exploit the impedimetric sensing of glucose if interfering agents are also present.

### Stability and Real Sample Analysis

The stability of the Pt/PANI-nfbD/GOx/Nf system was analyzed every week for 4 weeks, and the activity remained at 89% of the original activity for glucose additions of 1 m*M* each time and the electrode was stored at 4°C while not in use. The relative standard deviation was 2.8% for five successive measurements for 1 m*M* glucose, confirming that this sensor has a

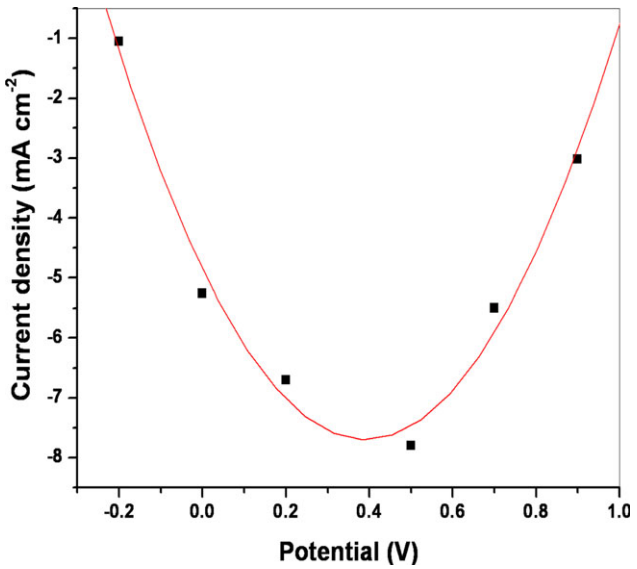


**Figure 14.** Current response of Pt/PANI-nfbD/GOx/Nf electrode to 1 m*M* glucose in PBS at 25° C for various potentials. [Color figure can be viewed in the online issue, which is available at wileyonlinelibrary.com.]

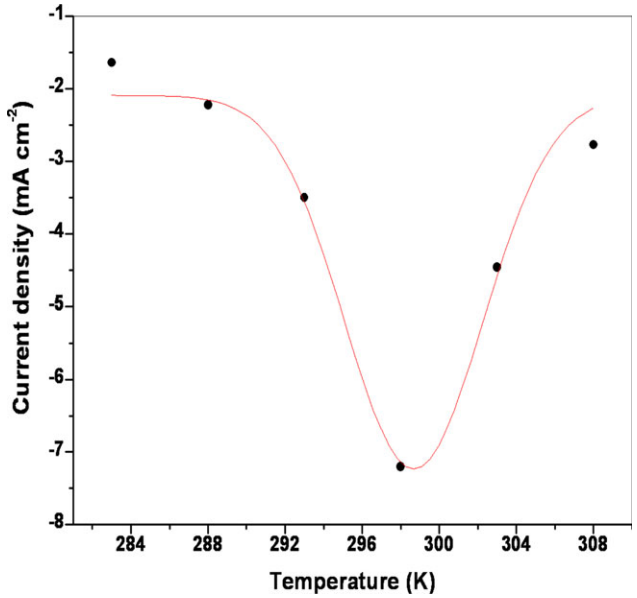


**Figure 15.** Current density of the enzyme immobilized Pt/PANI-nfbD/GOx/Nf electrode at various temperatures at 0.5 V. [Color figure can be viewed in the online issue, which is available at wileyonlinelibrary.com.]

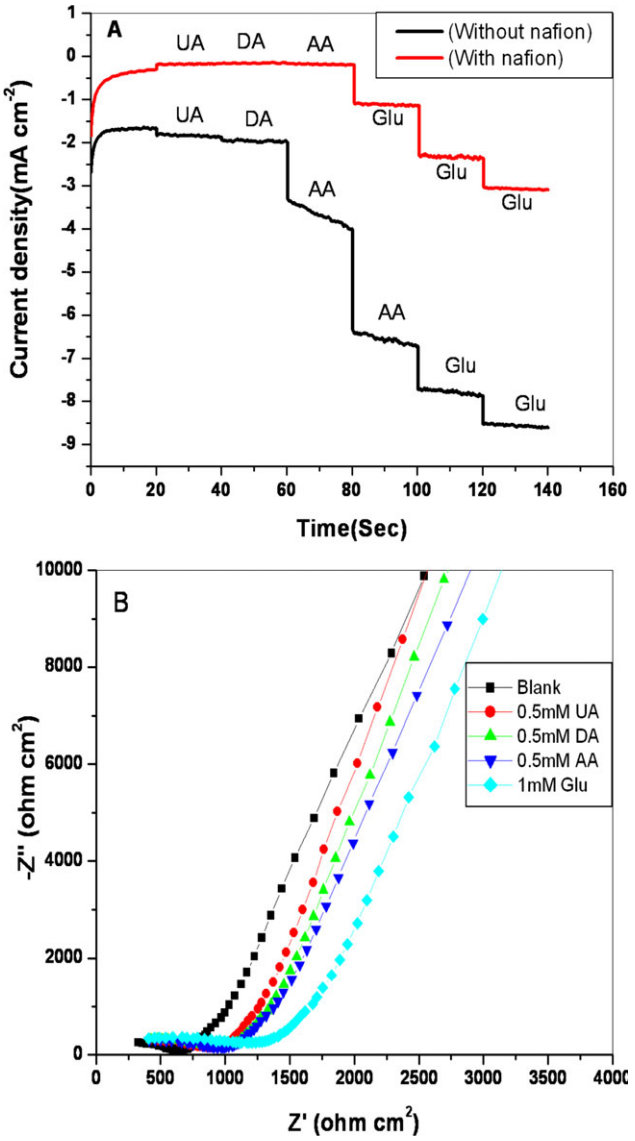


**Figure 16.** (A) Amperometric response of Pt/PANI-nfbD/GOx electrode with and without Nafion, upon addition of $5 \times 10^{-4}$ M each of UA, DA, and AA and successive additions of 1 m*M* glucose. (B) Nyquist plot for the Pt/PANI-nfbD/GOx/Nf electrode in blank solution (buffer 7 containing 0.5 m*M* glucose), and after addition of $5 \times 10^{-4}$ *M* each of UA, DA, and AA separately. [Color figure can be viewed in the online issue, which is available at wileyonlinelibrary.com.]

satisfactory reproducibility. For real sample analysis, venous blood without any anticoagulant agent was kept at constant temperature of 37°C. After centrifugation at 3000 rpm for 15 min, the blood serum of (diabetic) patients was collected and stored at 4°C for further use. The serum samples were analyzed with a Konelab automatic analyzer in the hospital. As can be seen from Table IV, the values measured by the present Pt/PANI-nfbD/GOx/Nf system and glucose automatic analyzer are consistent. These results indicate the suitability of the PANI nanofiber dendrites-modified glucose biosensor in practical applications.

**Table IV.** Estimation of Glucose in Blood Serum Samples

| Sample number | Value provided by the hospital (m*M*) | Predicted value (m*M*)[a] | Magnitude of the % error |
|---|---|---|---|
| 1 | 4.773 | 4.450 | 2.5 |
| 2 | 5.050 | 4.890 | 3.9 |
| 3 | 8.103 | 7.900 | 6.8 |
| 4 | 9.102 | 8.740 | 3.1 |

[a]Mean value of three trials.

## CONCLUSIONS

The simple electrochemical synthesis of PANI nanofiber dendrites using a potentiodynamic method with the help of *p*-toluene sulphonic acid as the dopant is demonstrated. The characterization of PANI has been carried out using FT-IR, UV–visible spectra, SEM, and TEM studies. Using amperometric and impedimetric techniques, the usefulness of this electrode for sensing of glucose is investigated. The equivalent circuit is constructed for fitting the Nyquist and Bode' plots, and the system parameters are obtained using MATLAB programming. The estimation of the Michaelis–Menten constant in conjunction with the calibration study demonstrates the satisfactory response of the electrode for the sensing of glucose. The interference of species such as AA, UA, and DA has been overcome by using a Nafion coating on the electrode.

## ACKNOWLEDGMENTS

The helpful comments of the reviewers are gratefully acknowledged. The authors also thank the IIT Madras hospital (Ms. Kani) for providing the blood serum samples for analysis. This work was supported by the Council of Scientific and Industrial Research, Government of India.

## REFERENCES

1. Wang, J. *Chem. Rev.* **2008**, *108*, 814.
2. Wang, Z.; Liu, S.; Wu, P.; Cai, C. *Anal. Chem.* **2009**, *81*, 1638.
3. Usman Ali, S. M.; Nur, M.; Willander, O.; Danielsson, B. *Sens. Actuators, B: Chem.* **2010**, *145*, 869.
4. Updike, S. J.; Hicks, G. P. *Nature* **1967**, *214*, 986.
5. Foulds, N. C.; Lowe, C. R. *Anal. Chem.* **1988**, *60*, 2473.
6. Janda, P.; Weber, J. *J. Electroanal. Chem.* **1991**, *300*, 119.
7. Hale, P. D.; Boguslavsky, L. I.; Karan, H. I.; Lan, H. L.; Lee, H. S.; Okamoto, Y.; Skotheim, T. A. *Anal. Chim. Acta.* **1991**, *248*, 155.
8. Zhao, C.; Meng, Y.; Shao, C.; Wan, L.; Jiao, K. *Electroanal.* **2008**, *20*, 520.
9. Tsai, T. W.; Heckert, G.; Neves, L. F.; Tan, Y.; Kao, D. Y.; Harrison, R. G.; Resasco, D. E.; Schmidtke, D. W. *Anal. Chem.* **2009**, *81*, 7917.
10. Dhand, C.; Sumana, G.; Datta, M.; Malhotra, B. D. *Thin Solid Films.* **2010**, *519*, 1145.

11. Cosnier, S.; Szunerits, S.; Marks, R. S.; Novoa, A.; Puech, L.; Perez, E.; Lattes, I. R. *Electrochem. Commun.* **2000**, *2*, 851.
12. Reddy, K. R. C.; Turcu, F.; Schulte, A.; Kayastha, A. M.; Schuhmann, W. *Anal. Chem.* **2005**, *77*, 5063.
13. Ye, J. S.; Wen, Y.; Zhang, W. D.; Gan, L. M.; Xu, G. Q.; Sheu, F. S. *Electrochem. Commun.* **2004**, *6*, 66.
14. Quinto, M.; Losito, I.; Palmisano, F.; Zambonin, C. G. *Anal. Chem.* **2000**, *367*, 692.
15. Brousseau, L. C.; Zhao, Q.; Shultz, D. A.; Feldheim, D. L. *J. Am. Chem. Soc.* **1998**, *120*, 7645.
16. Foulds, N. C.; Lowe, C. R. *J. Chem. Soc. Faraday Trans.* **1986**, *82*, 1259.
17. Pandey, P. C. *J. Chem. Soc. Faraday Trans.* **1988**, *84*, 2259.
18. MacDiarmid, A. G. *Angew. Chem. Int. Ed.* **2001**, *40*, 2581.
19. Brousseau, L. C.; Zhao, Q.; Shultz, D. A.; Feldheim, D. L. *J. Am. Chem. Soc.* **1998**, *120*, 7645.
20. Granot, E.; Basnar, B.; Cheglakov, Z.; Katz, E.; Wilner, I. *Electroanalysis.* **2006**, *18*, 26.
21. Huang, J.; Virji, S.; Weiller, B. H.; Kaner, R. B. *J. Am. Chem. Soc.* **2003**, *125*, 314.
22. Virji, S.; Huang, J.; Kaner, R. B.; Weiller, B. H. *Nano. Lett.* **2004**, *4*, 491.
23. Mi, H.; Zhang, X.; Yang, S.; Ye, X.; Luo, J. *Mater. Chem. Phys.* **2008**, *112*, 127.
24. Weng, S.; Lin, Z.; Chen, L.; Zhou, J. *Electrochim. Acta* **2010**, *55*, 2727.
25. Cui, Y.; Tang, D.; Liu, B.; Chen, H.; Zhang, B.; Chen, G. *Analyst.* **2012**, *137*, 1656.
26. Liu, C.; Hayashi, K.; Toko, K. *Sens. Actuators, B: Chem.* **2012**, *161*, 504.
27. Jia, W.; Su, L.; Lei, Y. *Biosens. Bioelectron.* **2011**, *30*, 158.
28. Ambrozic, G.; Djerdj, I.; Skapin, S. D.; Zigon, M.; Orel, Z. C. *Cryst. Eng. Comm.* **2010**, 12, 1862.
29. Ramya, R.; Sangaranarayanan, M. V. *J. Chem. Sci.* **2008**, *120*, 25.
30. Li, G.; Zhang, Z. *Macromolecules* **2004**, *37*, 2683.
31. Wang, J.; Chen, S. P.; Lin, M. S. *J. Electroanal. Chem.* **1989**, *273*, 231.
32. Furukawa, Y.; Ueda, F.; Hyodo, Y.; Harada, I.; Nakajima, T.; Kawagoe, T. *Macromolecules* **1988**, *21*, 1297.
33. Chen, S. A.; Lee, H. T. *Synth. Met.* **1992**, *47*, 233.
34. Kanungo, M.; Kumar, A.; Contractor, A. Q. *Anal. Chem.* **2003**, *75*, 5673.
35. Zhang, X.; Zhu, J.; Haldolaarachchige, N.; Ryu, J.; Young, D. P.; Wei, S.; Guo, Z. *Polymer* **2012**, *53*, 2109.
36. Liu, S.; Xu, H.; Ou, J.; Li, Z.; Yang, S.; Wang, J. *Mater. Chem. Phys.* **2012**, *132*, 500.
37. Varela, H.; Maranhao, S.; Mello, R. M. Q.; Ticianelli, E. A.; Torresi, R. M. *Synth. Met.* **2001**, *122*, 321.
38. Uygun, A.; Yavuz, A. G.; Sen, S.; Omastova, M. *Synth. Met.* **2009**, *159*, 2022.
39. Zhou, H.; Chen, H.; Luo, S.; Chen, J.; Wei, W.; Kuang, Y. *Biosens. Bioelectron.* **2005**, *20*, 1305.
40. Xue, H.; Shen, Z.; Li, Y. *Synth. Met.* **2001**, *124*, 345.
41. Gaikwad, P. D.; Shirale, D. J.; Savale, P. A.; Datta, K., Ghosh, P.; Pathan, A. J.; Rabbani, G.; Shirsat, M. D. *Int. J. Electrochem. Sci.* **2007**, *2*, 488.
42. Yi, Q.; Niu, F.; Yu, W. *Thin Solid Films.* **2011**, *519*, 3155.
43. Zhou, H. H.; Chen, H.; Chen, J. H.; Kuang, Y. F. *J. Cent. South. Univ. Technol.* **2006**, *13*, 653.
44. Garjonyte, R.; Malinauskas, A. *Biosens. Bioelectron.* **2000**, *15*, 445.
45. Retama, J. R.; Mecerreyes, D.; Lopez-Ruiz, B.; Lopez-Cabarcos, E. *Coll. Surf. A.* **2005**, *270–271*, 239.
46. Xu, J. J.; Chen, H. Y. *Anal. Chim. Acta.* **2000**, *423*, 101.
47. Shi, Q.; Wang, P.; Jiang, Y.; Kan, J. *Biocatal. Biotransform.* **2009**, *27*, 54.
48. Song, M. J.; Kim, J. H.; Lee, S. K.; Lee, J. H.; Lim, D. S.; Hwang, S. W.; Whang, D. *Microchim. Acta* **2010**, *171*, 249.
49. Santos, A. N.; Soares, D. A. W.; Alencar de Queiroz, A. A. *Mat. Res.* **2010**, *13*, 5.
50. Gursoy, S. S.; Uygun, A.; Tilki, T. *J. Macromol. Sci. Part A Pure Appl. Chem.* **2010**, *47*, 681.
51. Wang, J.; Myung, N. V.; Yun, M.; Monbouquette, H. G. *J. Electroanal. Chem.* **2005**, *575*, 139.
52. Zhang, H.; Zhong, H.; Yuan, R.; Chai, Y.; Li, W.; Zhong, X.; Zhang, Y. *Talanta* **2011**, *85*, 104.
53. Kang, X.; Mai, Z.; Zou, X.; Mo, J. *Anal. Biochem.* **2007**, *363*, 143.
54. Zhao, M.; Wu, X.; Cai, C. *J. Phys. Chem. C.* **2009**, *113*, 4987.
55. Xian, Y.; Hu, Y.; Liu, F.; Xian, Y.; Wang, H.; Jin, L. *Biosens. Bioelectron.* **2006**, 21, **1996**.
56. Gopalan, A. I.; Lee, K. P.; Ragupathy, D.; Lee, S. H.; Lee, J. W. *Biomaterials* **2009**, *30*, 5999.
57. Wan, D.; Yuan, S.; Li, G. L.; Neoh, K. G.; Kang, E. T. *ACS. Appl. Mater. Interfaces* **2010**, *2*, 3083.
58. Horng, Y. Y.; Hsu, Y. K.; Ganguly, A.; Chen, C. C.; Chen, L. C.; Chen, K. H. *Electrochem. Commun.* **2009**, *11*, 850.
59. McKubre, M. C. H.; Macdonald, D. D. In Measuring Techniques and Data Analysis, Impedance Spectroscopy: Theory, Experiment: Applications, 2nd ed.; Barsoukov, E., Macdonald, J. R., Eds.; Wiley: New York, **2005**; pp 20–533.
60. Feng, Y.; Yang, T.; Zhang, W.; Jiang, C.; Jiao, K. *Anal. Chim. Acta.* **2008**, *616*, 144.
61. Baur, J.; Gondran, C.; Holzinger, M.; Defranc, E.; Perrot, H.; Cosnier, S. *Anal. Chem.* **2010**, *82*, 1066.
62. Ramya, R.; Sangaranarayanan, M. V. *Sens. Actuators, B: Chem.* **2012**, *173*, 40.
63. Tlili, C.; Reybier, K.; Geloen, A.; Ponsonnet, L.; Martelet, C.; Ouada, H. B.; Lagarde, M.; Renault, N. *J. Anal. Chem.* **2003**, *75*, 3340.
64. Huang, Y.; Bell, M. C.; Suni, I. I. *Anal. Chem.* **2008**, *80*, 9157.
65. Katz, E.; Willner, I. (Review), *Electroanalysis* **2003**, *15*, 913.
66. Girija, T. C.; Sangaranarayanan, M. V. *Synth. Met.* **2006**, *156*, 244.
67. Vaidya, R.; Atanasov, P.; Wilkins, E. *Med. Eng. Phys.* **1995**, *17*, 416.